In vivo polymerization and manufacturing of wires and supercapacitors in plants

Eleni Stavrinidou[a,1], Roger Gabrielsson[a,1], K. Peter R. Nilsson[b], Sandeep Kumar Singh[a], Juan Felipe Franco-Gonzalez[a], Anton V. Volkov[a], Magnus P. Jonsson[a], Andrea Grimoldi[a], Mathias Elgland[b], Igor V. Zozoulenko[a], Daniel T. Simon[a], and Magnus Berggren[a,2]

[a]Laboratory of Organic Electronics, Department of Science and Technology, Linköping University, SE-601 74 Norrkoping, Sweden; and [b]Department of Chemistry, Physics and Biology, Linköping University, SE-581 83 Linkoping, Sweden

Edited by John A. Rogers, University of Illinois, Urbana, IL, and approved January 23, 2017 (received for review October 3, 2016)

Electronic plants, *e*-Plants, are an organic bioelectronic platform that allows electronic interfacing with plants. Recently we have demonstrated plants with augmented electronic functionality. Using the vascular system and organs of a plant, we manufactured organic electronic devices and circuits in vivo, leveraging the internal structure and physiology of the plant as the template, and an integral part of the devices. However, this electronic functionality was only achieved in localized regions, whereas new electronic materials that could be distributed to every part of the plant would provide versatility in device and circuit fabrication and create possibilities for new device concepts. Here we report the synthesis of such a conjugated oligomer that can be distributed and form longer oligomers and polymer in every part of the xylem vascular tissue of a *Rosa floribunda* cutting, forming long-range conducting wires. The plant's structure acts as a physical template, whereas the plant's biochemical response mechanism acts as the catalyst for polymerization. In addition, the oligomer can cross through the veins and enter the apoplastic space in the leaves. Finally, using the plant's natural architecture we manufacture supercapacitors along the stem. Our results are preludes to autonomous energy systems integrated within plants and distribute interconnected sensor–actuator systems for plant control and optimization.

electronic plants | in vivo polymerization | supercapacitor | conjugated oligomers

In the global energy cycle, plants are early converters of primary energy from the sun into chemical energy. They are indispensable for all of the herbivores, consumers, and predators as they are the initial source of food and nutrients, as well as the global regulator of atmospheric oxygen, water cycles, and climate (1). For mankind, plants are also appreciated as a source for heat, chemicals, fibers, and bulk materials, and are used in a wide range of consumer, societal, technological, and industrial applications. Traditionally, in the forest industry and agriculture, a vast array of fertilizers is used to improve plant growth, performance, and production. More recently, most sophisticated methods for altering and optimizing plant functions are based on genetic engineering (2). Deploying fertilizers and gene-modified plants in agriculture can be very restrictive because undesired chemicals and species can "leak" into—and potentially pollute—nature. As an alternative to genetic modification, smart materials such as carbon nanotubes (3) and inorganic nanoparticles (4, 5), have been introduced into the tissue and constructs of plants to enhance and regulate their functions.

Plants are renewable, large-volume, and high-performing machineries that represent an untapped source for the production of advanced materials, electronics, and energy technology. Furthermore, a distributed technology integrated within plants, which could sense phytohormones (6) and their metabolites (7) and then actuate functions, would be ideal to autoregulate and optimize growth and overall functions. One strategy to further advance plants as technological systems, and to dynamically control their physiology, would be to manufacture integrated electronic systems that selectively convert chemical compounds into electric signals and energy, and vice versa, at a high spatiotemporal resolution. Integrated electronic systems are typically composed of contacts, wires, interconnects, and components. Recently, we introduced the concept of electronic plants (*e*-Plants), an organic bioelectronic technology capable of forming analog and digital circuits inside the leaves and xylem vascular tissue of *Rosa floribunda*, respectively (8). From a circuit perspective, forming a biofuel cell technology or a sensor-and-actuator system integrated inside a living plant would require electronic charge transport over long distances (wires) and charge storage with low electrical loss (capacitors).

Self-organization of materials within the internal structure of the plant is a key aspect of *e*-Plant technology. As a first example we have used PEDOT-S [alkoxysulfonate-functionalized poly(3,4-ethylenedioxythiophene)] (9), a self-doped p-type conducting polymer, to fabricate conducting wires along the xylem vascular tissue of the plant, leveraging the natural process of transpiration to distribute materials. PEDOT-S self-organized in the xylem, the vascular tissue which transports water and nutrients upwards in the plant, and formed hydrogel-like conducting wires along the stem (8). Using the xylem-wires and the surrounding cellular and extracellular domains, we constructed organic electrochemical transistors and simple digital circuits. Several of our previous attempts, based on other conducting polymers or in vivo chemical- or electro-polymerization of monomers, failed either due to clogging at the inlet (e.g., at the stem cutting), toxicity, or resulted in

Significance

Plants with integrated electronics, *e*-Plants, have been presented recently. Up to now the devices and circuits have been manufactured in localized regions of the plant due to limited distribution of the organic electronic material. Here we demonstrate the synthesis and application of a conjugated oligomer that can be delivered in every part of the vascular tissue of a plant and cross through the veins into the apoplast of leaves. The oligomer polymerizes in vivo due to the physicochemical environment of the plant. We demonstrate long-range conducting wires and supercapacitors along the stem. Our findings open pathways for autonomous energy systems, distributed electronics, and new *e*-Plant device concepts manufactured in living plants.

Author contributions: E.S., R.G., I.V.Z., D.T.S., and M.B. designed research; E.S., R.G., K.P.R.N., S.K.S., J.F.F.-G., A.V.V., and M.P.J. performed research; R.G. contributed new reagents/analytic tools; E.S., R.G., K.P.R.N., S.K.S., J.F.F.-G., A.V.V., A.G., and M.E. analyzed data; and E.S., D.T.S., and M.B. wrote the paper.

The authors declare no conflict of interest.

This article is a PNAS Direct Submission.

Freely available online through the PNAS open access option.

[1]E.S. and R.G. contributed equally to this work.

[2]To whom correspondence should be addressed. Email: magnus.berggren@liu.se.

This article contains supporting information online at www.pnas.org/lookup/suppl/doi:10.1073/pnas.1616456114/-/DCSupplemental.

only localized polymerization. To gain more versatility of device fabrication, *e*-Plant technology requires new materials that can be distributed in every part of the plant (not only in the stem, as in the case of PEDOT-S) without adversely affecting or terminating the natural physiological processes of the plant. For example, electronic connection between the roots and stem with the photosynthetic centers in the leaves and reproductive organs in flowers would provide a range of new capabilities for using and deploying *e*-Plant technology.

Rational molecular design of materials provides the solution to many technological bottlenecks, as materials can be custom-made to meet the demands for a specific application or performance criteria. To address the *e*-Plant bottleneck of "long-range" root-to-leaf or root-to-flower connectivity, water-soluble conjugated oligomers that can self-organize and polymerize in the plant's internal structures upon distribution would be an ideal solution. In this work we report the design, synthesis, and application of just such a water-soluble conjugated oligomer: sodium salt of bis[3,4-ethylenedioxythiophene]3thiophene butyric acid, ETE-S, where 3,4-ethylenedioxythiophene (EDOT) moieties have been inserted as external end groups to thiophene butyric acid (Fig. 1*A*). Adding EDOT units in hybrid oligothiophenes results in molecules with lower oxidation potential (10) while at the same time we overcome the synthetic difficulties of pure EDOT oligomers. Due to its small molecular size and functionality, the oligomer can be distributed to every part of the xylem vascular tissue of an *R. floribunda* cutting, from the stem, through petioles, to leaves and flowers, and self-organizes to form long-range conducting wires. In addition, the ETE-S can cross through the veins and enter the apoplastic space in the leaves. Finally, we leverage the electrical and charge-capacity properties of the resulting xylem wires and electrodes to demonstrate supercapacitors along the stem.

Results and Discussion

ETE-S was dissolved in deionized (DI) water (1 mg/mL) and a rose cutting with a fresh cross-section cut was immersed in the solution for ~24 h. During this time the ETE-S solution was transported apically through the xylem water transport channels via the plant's natural transpiration process. Two hours after the immersion of the rose in solution, the xylem in the vascular bundles that were exposed appeared to be darker, indicating initiation of the polymerization process. It must be noted that the ETE-S solution exterior to the plant did not polymerize at the same rate as the ETE-S in the vascular tissue of the plant. After 24 h of immersion, the rose was removed and rinsed with water (Fig. 1 *B*, *i*). By peeling off the outer bark, cortex, and phloem, dark continuous lines were exposed along the entire length of the stem (>10 cm). Fig. 1 *B*, *ii* and Fig. 1 *B*, *iii* show cross-sections at the bottom part of the stem, and at the top part of the stem, just below the flower. The xylem tissue has a dark color, suggesting that the ETE-S has been transported and polymerized from the bottom to the top of the stem. SEM and optical microscopy further indicate that, in some cases, xylem vessels are entirely filled, while in others, the longer oligomers and polymer coats the inner walls (*SI Appendix*, Fig. S1). The xylem vascular tissue extends through every part of the plant, from the roots, via the stem, to the leaves and flowers. Fig. 1 *B*, *iv–vi* shows optical micrographs of the petal veins, the main vascular bundle of the

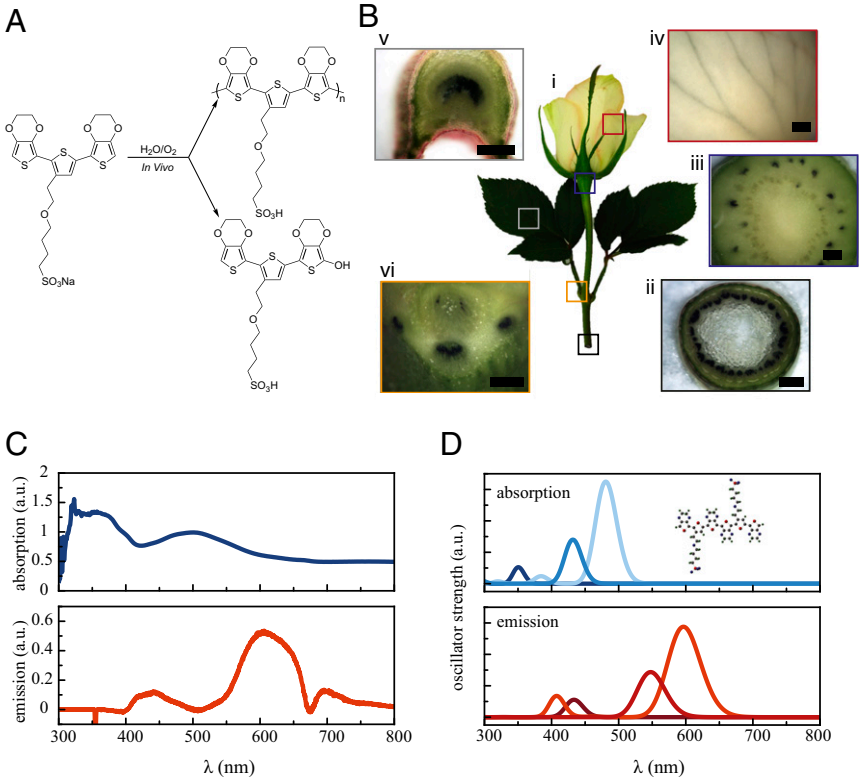

Fig. 1. ETE-S distribution and polymerization in a rose cutting. (*A*) Synthetic route/polymerization of ETE-S in vivo. (*B*, *i*) Rose after immersion in ETE-S aqueous solution for 24 h. (*B*, *ii–iii*) Bottom and top cross-section of stem with vascular bundles darkened due to polymer deposition. (Scale bar, 1 mm.) (*B*, *iv*) White rose petal with polymer-darkened veins. (Scale bar, 1 mm.) (*B*, *v–vi*) Leaf stem and petiole with polymer-darkened vascular bundles. (Scale bar, 0.5 mm and 1 mm, respectively.) (*C*) Absorption and emission spectra of polymer-filled xylem (after DMSO extraction), the latter using laser excitation at 355 nm. (*D*) Theoretical calculation of absorption and emission spectra for ETE-S molecule, hexamer (2 ETE-S units) and dodecamer (4 ETE-S units) (from dark to light color). (Inset) Structure of the hexamer.

leaf, and the vascular bundles of the petiole. ETE-S appears to travel through the entire xylem system of the rose cutting, polymerizing to form coatings and wires. Even in the case where leaves are separated more than 10 cm from the stem by the petioles, ETE-S is effectively transported and polymerized in their vascular tissue.

The conductivity of polymerized ETE-S wires was measured using two Au probes applied into individual filled xylem wires along the stem. The measured conductivity of the ETE-S-based wires was 7.25 ± 3.38 S/cm (n = 17) (*SI Appendix*, Figs. S2 and S3). In comparison, PEDOT-S xylem wires typically exhibit two orders of magnitude lower conductivity (8). The high conductivity was retained even for centimeter-long wires, showing that considerable conductivity could be achieved over extended distances along the xylem wires. To get a molecular description of the ETE-S morphology and elucidate this long-range conductivity, we performed molecular dynamics (MD) simulations. A characteristic snapshot of the structure is shown in *SI Appendix*, Fig. S4. The MD simulations show that oligo-ETE-S chains π–π stack in crystallites which can be linked in three different ways: interpenetrating chains, interconnecting aliphatic chains through the sulfate group, or π–π interactions between chains belonging to different crystallites. Taken together, these interactions result in percolative paths through the crystallites, which support conductivity. To elucidate the degree of polymerization of the ETE-S distributed in the plant, we extracted material from the xylem and characterized its chemical composition and photophysical properties. Pieces of xylem filled with the ETE-S-based material were mechanically crushed in dimethyl sulfoxide (DMSO) solvent. Fig. 1*C* shows the absorption and emission spectra for a typical xylem wire extract, after subtraction of the spectral contribution from the plant tissue. The ETE-S oligomer exhibits an absorption band at 357 nm and emission at 448 nm (spectra recorded for 0.1 mg/mL in DMSO solution; *SI Appendix*, Fig. S5). The ETE-S peak is present in the xylem-wire extract, suggesting the presence of nonpolymerized molecules in the vascular tissue. To reveal the origin of the absorption and emission features found at relatively longer wavelengths, we investigated ETE-S structures using time-dependent density functional theory (DFT) modeling. The theoretical calculations are used to identify the length and excitation state of oligomers by comparing the calculated photophysical properties with experimental observation (11, 12). DFT analysis of the neutral ETE-S species (Fig. 1*D*) revealed strong highest occupied molecular orbital–lowest occupied molecular orbital transitions at 350 nm for absorption and at 433 nm for emission spectra. These transitions saturate toward higher wavelengths at 481 nm for optical absorption and 597 nm for emission, as the length of the polymer chain increases to dodecamer and beyond. The recorded absorption and emission peaks of the xylem extracts were found around 500 nm and 600 nm, respectively, suggesting that ETE-S polymerizes within the plant and forms polymer chains of 4 and more ETE-S units. The experimental transition at 800 nm (full spectra shown in *SI Appendix*, Fig. S6) indicates the presence of polaron and bipolaron charge carriers in the polymer.

To further investigate the composition of the xylem wire extracts, we performed liquid chromatography-mass spectrometry (LC-MS) coupled with a diode array detector (DAD), and ^{1}H-NMR spectroscopy. The LC-MS data show the presence of ETE-S molecules, hexamers (2 ETE-S units), and fragments of larger length (*SI Appendix*, Fig. S7). The coupled DAD function allows us to have a UV-VIS signature on the detected fragments. In this case, only the ETE-S and the hexamers show UV-VIS signatures in agreement with the theoretical calculations (Fig.1*D*), whereas the larger fragments do not exhibit any absorption. Conversely, the NMR data (*SI Appendix*, Fig. S8) show the possibility of oligo-ETE-S composed of at least 3 units of ETE-S (nonamer). In addition, we observe proton signals between 8 and 9 ppm from the aromatic region, suggesting labile proton sites that support a polymerization reaction through oxygen reduction within the xylem of the plant.

ETE-S solution with and without immersed pieces of plant tissue were analyzed using UV-Vis absorption spectrometry to investigate the role of plant tissue or plant compounds on the polymerization. The solution that contained the plant tissue polymerized faster than the solution without tissue (*SI Appendix*, Fig. S9). This result indicates that the plant releases one or more chemical species that catalyze the polymerization, increasing the reaction rate beyond what is promoted by air oxidation. In addition, after 18 h of immersion of the pieces of plant tissue in the solution, the polymerization of the ETE-S oligomer was primarily localized on the xylem even though the whole tissue was exposed to the ETE-S solution (*SI Appendix*, Fig. S10), indicating preferential absorption of the ETE-S on the xylem surface. Enhanced polymerization could also be observed along the cuts in the plant tissue localized around bark and phloem vascular tissue. It is known that wounded regions of the plant release reactive oxygen species (ROS) as a defense response (13), and these ROS may act as catalysts for the polymerization reaction.

It is clear that polymerization of the ETE-S in the plant is promoted by the local physicochemical environment present in the xylem vessels. Lignin, one of the main components of the xylem, is hydrophobic and should favor the interaction with the backbone of the ETE-S—an interaction that is further aided by the confined space of the vessel. We hypothesize that the ETE-S oligomer appears as weak pathogen to the sophisticated defense system of the plant, which triggers the generation of ROS. Subsequently, ROS are released from the parenchyma cells to the adjacent xylem vessels and catalyze the polymerization reaction (14). The observation of labile protons in the NMR spectra and the presence of oligo-ETE-S further support the hypothesis that ROS catalyzes ETE-S polymerization in plants. Therefore, the reaction is a one-pot, aqueous-based oxidation catalyzed by ROS inside the xylem.

Polymerization of ETE-S is clearly localized in the xylem vessels. However, the ETE-S molecule was able to pass the xylem walls and enter into the apoplastic pathway of the leaves, finally reaching the spongy mesophyll compartments (Fig. 2*A*). This is the same route followed by water molecules during normal transpiration. Dyes like brilliant blue (793 g/mol) and indigo carmine (466 g/mol) have molecular weights similar to ETE-S (544 g/mol) and are commonly used as dyes in the flower industry because they can pass the xylem vessels and enter the apoplast, thus coloring leaves and flowers. Fig. 2*B* shows confocal fluorescence images of a leaf attached to a rose cutting immersed in ETE-S solution for ∼24 h, together with an image of a negative control leaf attached to a rose cutting immersed in tap water (Fig. 2*C*). The blue color in the fluorescence images corresponds to emission from 424 to 500 nm whereas the green color covers the spectrum from 510 to 607 nm. From the images and the recorded spectra, shown in Fig. 2*D*, we conclude that the functionalized rose leaf exhibits additional fluorescence in the range of 424–500 nm (Fig. 2*C*). By comparing these spectra with the theoretical and experimental emission spectra of the ETE-S molecule and its polymer, the additional fluorescence can be attributed to ETE-S molecules. As a positive control, leaves were vacuum-infused (8) with freshly prepared ETE-S solution and analyzed by confocal fluorescence microscopy. With this method we ensure the ETE-S solution is delivered in the apoplast of the leaf through the stomata. The resulting positive control spectra were similar to those from leaves functionalized with ETE-S through the stem (*SI Appendix*, Fig. S11). This capability of ETE-S to arrange into electronic material, delivered into the vascular tissue in the stem, and extending into the leaf apoplast, creates opportunities to derive distributed *e*-Plant circuits connecting in vivo manufactured devices located in different components of

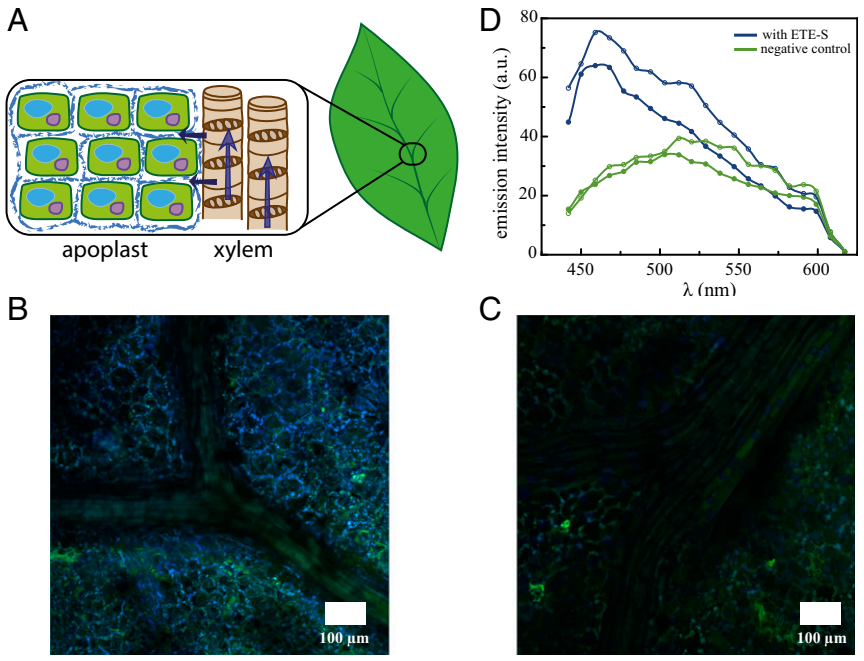

Fig. 2. Distribution of ETE-S from the stem to the veins and extracellular space of leaves. (*A*) Schematic showing the transport path from the xylem vessels in the leaf to the apoplast and spongy mesophyll. (*B*) Confocal fluorescent image of leaf functionalized with ETE-S and (*C*) without functionalization (negative control). (*D*) Spectra from selected locations on a leaf with (blue) and without (green) ETE-S upon excitation with 405-nm laser.

the plant. Electronic circuitry in the veins combined with biofunctionalized molecules in the leaf are preludes to energy-harvesting devices, sensors, and localized addressing components for plant control and optimization.

Indeed, new routes toward energy harvesting are one of the main visions for *e*-Plant technology. Other direct or indirect strategies are exemplified by the extraction of photosynthetic current using nanoprobes (15) and microbial fuel cells that use the organic substances released from roots (16). A more versatile approach will require an autonomous system where energy conversion, and storage coexist in the same plant. Toward this end, we explored the xylem wires for supercapacitor applications.

Plants' anatomy provides an ideal architecture for developing supercapacitors in vivo; long-range conducting xylem wires are parallel, physically isolated from each other, and are surrounded with cellular domains and extracellular space rich in electrolyte. Two parallel ETE-S based polymer xylem wires served as separate electrodes (redox electrodes and collectors) and the plant tissue in between them served as the electrolyte separator. Two Au probes defined the electrode contacts. Fig. 3 shows a simplified schematic illustration of the general structure, configuration, and wiring of the supercapacitor experiment, along with the optical micrograph of the corresponding supercapacitor formed in vivo.

Characterization of a typical device is presented in Fig. 3 *C*–*E*. In Fig. 3*C* we show galvanostatic charging and discharging for I = 0.25–1 μA. The supercapacitor is stable over 500 cycles during galvanostatic cycling with I = 0.5 μA. To extract the capacitance and the equivalent series resistance (ESR) we fit the galvanostatic discharging curves with the response of a simple R,C in series circuit. The capacitance and the ESR remain constant over the cycling with values of C = 73 μF and ESR = 33 kΩ. As a merit of charge retention we have calculated the coulombic efficiency (CE) of the device. The CE increases after initial cycling and reaches a value of 0.99, showing excellent charge retention. The voltage of the devices after 1 h of self-discharge drops by 50–70% of the initial one (*SI Appendix*, Fig. S12). The frequency dependence of the device was characterized with electrochemical impedance spectroscopy and its response was modeled with an equivalent circuit (*SI Appendix*, Fig. S13). Although in the ideal case the model should consist of a resistor in series with a capacitor as in the case of the galvanostatic model, here we use a more complex model to fit the data. The capacitive behavior of the device is modeled by a constant phase element (CPE). The ESR is expressed by the resistive shift on the onset of the CPE response. The equivalent circuit contains additional elements where a physical origin cannot be attributed with certainty. Having in mind the complex structure of the xylem tissue, the additional elements can be the result of charge transfer and charging of the interphases. To extract the specific capacitance of the oligo-ETE-S xylem electrodes, devices with various dimensions (electrode volumes) were analyzed. Although the xylem, as any biological tissue, has complex geometry, we approximate its geometry with a cylinder and measure the dimensions of each xylem wire from optical microscopy images. Xylem wires have a typical diameter of 30–50 μm, and lengths on the scale of centimeters. Fig. 3*F* shows the capacitance per area (cross-section of the xylem wire) versus electrode length. The slope of the resulting linear relationship yields the specific capacitance, equal to 20 F/cm^3, a value in the typical range for conducting polymers (17). The fact that the capacitance/area scales linearly with the length of the xylem electrodes confirms that the entire volume of the wire contributes to charge storage (18, 19). As the polymer is doped or dedoped, ions move in and out of the bulk material, resulting in a pseudocapacitive charge storage reaction. These ions are able to penetrate the material, resulting in a volumetric capacitance, in contrast to metal electrodes, where the capacitance is limited by the double layer and hence the area of the electrode. The most charge that we were able to store in the xylem capacitors was 0.65 mC, with a corresponding capacitance of 0.25 mF. In this case, the length of the continuous oligo-ETE-S wire was 1.7 cm, assuming that the specific capacitance was constant. Further increase of the total capacitance of xylem supercapacitors could be achieved by connecting several xylem wires in parallel.

Conclusions

High-performance conducting wires and electrodes, with a conductivity up to 10 S/cm and a specific capacitance of 20 F/g, have

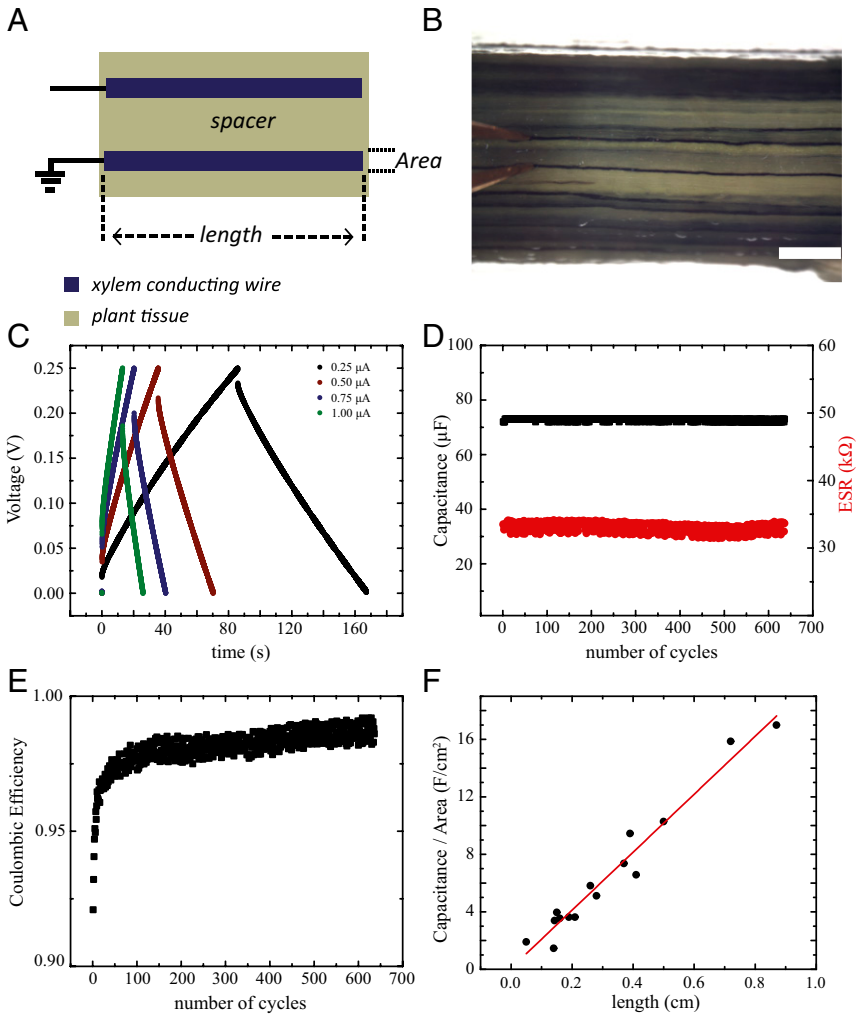

Fig. 3. Plant supercapacitor. (*A*) Simplified schematic and wiring of a plant supercapacitor where the xylem wires comprise the electrodes, and the plant tissue in between comprises the electrolytic spacer. (*B*) Optical micrograph of a rose supercapacitor. (Scale bar, 1 mm.) (*C*) Typical charging–discharging curves for a rose supercapacitor. (*D*) Capacitance and equivalent series resistance and (*E*) CE of a typical supercapacitor over galvanostatic cycling of the device, for I = 0.5 μA and V_{max} = 0.25 V. (*F*) Capacitance per area versus length of xylem limiting wire.

been in vivo polymerized from the custom-synthesized ETE-S in *R. floribunda*. We have used the natural physiology and response mechanisms of the xylem vascular tissue as the tubular template and catalyst, respectively, to achieve long-range electrical conductors and extended supercapacitors. These findings pave the way for combining charge storage devices with energy conversion technology—also manufactured inside plants—to derive autonomous systems for a future "green" energy harvesting technology, i.e., "power plants" or "flower power" technology. The long-range conductivity afforded by ETE-S also allows for sensors and delivery devices (actuators) to be distributed and interconnected throughout the entire plant for electronic autoregulation of plant physiology and defense mechanisms.

Materials and Methods

All data are available upon request to the authors.

Chemical Synthesis of ETE-S Is Reported in the *SI Appendix*.

Oligo-ETE-S wire formation in rose xylem and conductivity measurement. We used the method for in vivo wire formation and characterization as previously described (8). Briefly, we used stems of *R. floribunda* purchased from a local flower shop. The stems were kept in water and under refrigeration until they were used for the experiment. The stems were cleaned with tap water and then a fresh cut was made to the bottom of the stem with a sterilized scalpel under DI water. The stem was then immersed in 1 mg/mL ETE-S in DI water, and kept at ∼40% humidity and 23 °C for ∼24 h. During the absorption, fresh 2–3-mm cuts to the bottom of the stem were done every 12 h. After absorption, the stems were kept refrigerated in DI water until used for characterization and device fabrication. For conductivity measurements, the bark and phloem were peeled off to reveal the xylem. The stem was mounted on a Petri dish using UHU Patafix. The exposed xylem tissue was surrounded by DI water to prevent drying out during the experiment. For all of the measurements, Au-plated tungsten probe tips (Signatone SE-TG) with a tip diameter of 10 μm were used. Using micromanipulators and viewing under a stereo microscope (Nikon SM Z1500), the probe tips were brought into contact with the wire, and a very small pressure was applied in order for the tips to penetrate the xylem and make contact with the oligo-ETE-S inside. Conductivity measurements were performed on wires of various lengths and the dimensions of the wire (length and diameter) were measured from optical microscopy images using ImageJ. Electrical measurements were made using a Keithley 2602 SourceMeter controlled by a custom LabVIEW program. The voltage was swept from 0.5 to −0.5 V with a rate of 50 mV/s.

ETE-S–based material extraction from plant and photophysical characterization. To extract the polymer from the xylem, the stem was dissected using a scalpel to prepare xylem tissue in smaller pieces. Then, using a mortar and pestle, these small pieces of xylem tissue were mechanically crushed in DMSO. Upon mechanical crushing, the DMSO acquired a pink–purple coloration. As a control, the same procedure was done on xylem tissue that had not absorbed ETE-S. In this case, the DMSO solution acquired a green color. The xylem

tissue in DMSO was collected with a pipette and characterized. In both the ETE-S and control cases, the same amount of xylem tissue and DMSO solvent was used. The UV-Vis spectra (300-1,300 nm, step 1 nm) were taken using a PerkinElmer Lambda 900 spectrometer.

For emission spectra, the same solutions were used upon dilution. For excitation we used the 355-nm output beam of a pulsed neodymium-doped yttrium aluminum garnet laser (Tempest 10, New Wave Research), filtered through a 355-nm laser line filter (Thorlabs). Light emitted from the solutions was captured orthogonally to the excitation beam using a liquid light guide (Newport model 77569), and sent to a spectrometer (Shamrock 303i, Newton detector, Andor Technology).

It must be noted that although the mass of xylem and DMSO solvent was the same in the sample and control, it was possible to have variation of the plant tissue contribution between the two solutions. Nevertheless, the features that appear due to the ETE-S material are reproducible and not negligible in any case.

MD simulations. MD simulations were performed to describe the morphology of ETE-S. Oligomer chains of a length of 2 ETE-S molecules were used in the calculations, where each aliphatic chain included a negatively charged sulfate group. Then, sodium cations (Na^+) were used as counterions to get a neutral molecular system. ETE-S chains and Na^+ cations were solvated with water, where a concentration ~0.09 M of ETE-S was obtained. All of the molecules were initially randomly placed in a solvent box and the system was described by the all-atom general Amber force field (20) and the extended simple point charge model (21) for water. The system was then minimized and equilibrated for a 20-ns production run. As the main result, a crystal nucleation takes places in the solution such that aggregates crystallized as π–π stacks of ETE-S chains were obtained. Self-doped configurations such that the sulfate groups are linked to the backbone chain or cross-linked to the closest neighbor chain were also observed, and are shown in *SI Appendix*, Fig. S4.

DFT calculation for ETE-S, (ETE-S)$_2$, and (ETE-S)$_4$. All time-dependent DF calculations were carried out using GAUSSIAN 09 (22). Range-separated hybrid functional ωB97XD (23) /6–31+g(d) level of theory was used, which includes 22% Hartree–Fock (HF) exact exchange at short range and 100% HF exact exchange at long range, with additional Grimme's D2 (24) dispersion correction. The solvent effect was included by using the polarizable continuum model (25) as implemented in the GAUSSIAN package.

Confocal microscopy on leaves with ETE-S and control. Leaves that had been attached to a rose that absorbed ETE-S aqueous solution for 24 h were detached and refrigerated. Before characterization with the confocal microscope, they were cut in 1–2-cm^2 pieces and were mounted on a microscope slide using Dako (fluorescent mounting medium, Agilent Pathology solutions) with the abaxial side facing the objective. The same procedure was performed for the positive and negative control leaves. Images and emission spectra were acquired using an inverted LSM 780 confocal microscope (Carl Zeiss) with excitation wavelength at 405 nm.

Xylem supercapacitor device fabrication and characterization. The electrodes of the supercapacitor were defined by two parallel xylem wires. The spacer of the supercapacitor was defined by the liquid-filled plant tissue between the wires. Contact with the electrodes was made using Au-plated tungsten probe tips. The supercapacitor was characterized by galvanostatic charging and discharging. The absolute value of charging currents was kept equal to the discharging one. Devices were switched from charging to discharging as soon as the set maximum voltage (0.25 V) was reached. Voltage was recorded with a sampling interval of 10 ms.

A simple equivalent circuit of R,C in series was used to fit the discharging response of the supercapacitor. The resistor represents the equivalent series resistance.

The device capacitance C, the ESR, and the CE were extracted using the following relations:

$$C = I/(dV/dt),$$

where I is the applied current, and dV/dt is the slope of the discharge curve as done in standardized characterization of supercapacitors (IEC 62576).

$$\mathrm{ESR} = \Delta V/2I,$$

where I is the applied current and ΔV the sudden voltage drop at the beginning of the discharging curve.

$$\mathrm{CE} = \mathrm{Qdischarging}/\mathrm{Qcharging},$$

where Qdischarging (Qcharging) is the charge that is released (stored) by the supercapacitor. Qdischarging (Qcharging) was calculated integrating the discharging (charging) current over the discharge (charge) time $Q = \int I\,dt$.

For calculation of the specific capacitance the dimension of the limiting wire (e.g., shorter of the two) was measured from microscopy images using ImageJ. In some cases, we defined the length of the limiting wire by cutting a section of the xylem wire. All electrical measurements were performed using a Keithley 2602 with a custom LabVIEW program. The analysis of the data was performed using MATLAB and ORIGIN.

ACKNOWLEDGMENTS. The authors acknowledge Prof. Ove Nilsson (Umeå Plant Science Center) and Dr. Simone Fabiano (Linköping University) for fruitful discussions. This project was funded primarily by a Knut and Alice Wallenberg Foundation Scholar Grant to M.B. (KAW 2012.0302). Additional funding was provided by Linköping University, the Önnesjö Foundation, the Wenner-Gren Foundations, and the Swedish Government Strategic Research Area in Materials Science on Functional Materials at Linköping University (Faculty Grant SFO-Mat-LiU 2009 00971). E.S. is also supported by a Marie Sklodowska Curie Individual Fellowship (MSCA-IF-EF-ST, Trans-Plant, 702641).

1. Raven PH, Evert RF, Eichhorn SE (2005) *Biology of Plants* (Freeman, New York), pp 2–15.
2. Liu W, Yuan JS, Stewart CN, Jr (2013) Advanced genetic tools for plant biotechnology. *Nat Rev Genet* 14(11):781–793.
3. Giraldo JP, et al. (2014) Plant nanobionics approach to augment photosynthesis and biochemical sensing. *Nat Mater* 13(4):400–408.
4. Djikanović D, et al. (2012) Interaction of the CdSe quantum dots with plant cell walls. *Colloids Surf B Biointerfaces* 91:41–47.
5. Masarovicova E, Kralova K (2013) Metal nanoparticles and plants. *Ecol Chem Eng S* 20:9.
6. Santner A, Calderon-Villalobos LI, Estelle M (2009) Plant hormones are versatile chemical regulators of plant growth. *Nat Chem Biol* 5(5):301–307.
7. Ruan Y-L (2014) Sucrose metabolism: Gateway to diverse carbon use and sugar signaling. *Annu Rev Plant Biol* 65(August):33–67.
8. Stavrinidou E, et al. (2015) Electronic plants. *Sci Adv* 1(10):e1501136.
9. Karlsson RH, et al. (2009) Iron-catalyzed polymerization of alkoxysulfonate-functionalized poly (3, 4-ethylenedioxythiophene) of high conductivity. *Chem Mater* 21: 1815–1821.
10. Turbiez M, et al. (2005) Design of organic semiconductors: Tuning the electronic properties of pi-conjugated oligothiophenes with the 3,4-ethylenedioxythiophene (EDOT) building block. *Chemistry* 11(12):3742–3752.
11. Salzner U (2008) Investigation of charge carriers in doped thiophene oligomers through theoretical modeling of their UV/Vis spectra. *J Phys Chem A* 112(24):5458–5466.
12. Salzner U, Aydin A (2011) Improved prediction of properties of π-conjugated oligomers with range-separated hybrid density functionals. *J Chem Theory Comput* 7(8):2568–2583.
13. Baxter A, Mittler R, Suzuki N (2014) ROS as key players in plant stress signalling. *J Exp Bot* 65(5):1229–1240.
14. Yadeta KAJ, J Thomma BP (2013) The xylem as battleground for plant hosts and vascular wilt pathogens. *Front Plant Sci* 4(April):97.
15. Ryu W, et al. (2010) Direct extraction of photosynthetic electrons from single algal cells by nanoprobing system. *Nano Lett* 10(4):1137–1143.
16. De Schamphelaire L, et al. (2008) Microbial fuel cells generating electricity from rhizodeposits of rice plants. *Environ Sci Technol* 42(8):3053–3058.
17. Snook GA, Kao P, Best AS (2011) Conducting-polymer-based supercapacitor devices and electrodes. *J Power Sources* 196(1):1–12.
18. Proctor CM, Rivnay J, Malliaras GG (2016) Understanding volumetric capacitance in conducting polymers. *J Polym Sci Part B Polym Phys* 54:1433–1436.
19. Malti A, et al. (2015) An organic mixed ion-electron conductor for power electronics. *Adv Sci (Weinh)* 3(2):1500305.
20. Wang J, Wolf RM, Caldwell JW, Kollman PA, Case DA (2004) Development and testing of a general Amber force field. *J Comput Chem* 25(9):1157–1174.
21. Berendsen HJC, Postma JPM, van Gunsteren WF, Hermans J (1981) Interaction models for water in relation to protein hydration. *Intermolecular Forces: Proceedings of the Fourteenth Jerusalem Symposium on Quantum Chemistry and Biochemistry*, ed Pullman B (Springer, Dordrecht, The Netherlands), pp 331–342.
22. Frisch MJ, et al. (2009) GAUSSIAN 09, Revision E.01 (Gaussian, Inc., Wallingford, CT).
23. Chai J-D, Head-Gordon M (2008) Long-range corrected hybrid density functionals with damped atom-atom dispersion corrections. *Phys Chem Chem Phys* 10(44):6615–6620.
24. Grimme S (2006) Semiempirical GGA-type density functional constructed with a long-range dispersion correction. *J Comput Chem* 27(15):1787–1799.
25. Tomasi J, Mennucci B, Cammi R (2005) Quantum mechanical continuum solvation models. *Chem Rev* 105(8):2999–3093.